Materials Advances

ROYAL SOCIETY OF CHEMISTRY

PAPER

View Article Online
View Journal

Cite this: DOI: 10.1039/d5ma01450f

Light-triggered and nanocarrier properties of nitrogen-doped carbon nanodots

Ludovica Maugeri,†[a] Grazia Maria Letizia Consoli,†[b] Giuseppe Forte,[a] Giorgia Fangano,[a] Loredana Ferreri,[b] Giuseppe Granata,[b] Paolo Giuseppe Bonacci,[ce] Nicolò Musso,[de] Luca Lanzanò,[f] Elisa Longo,[f] Marcello Marelli,[g] Angelo Ferlazzo,[h] Antonino Gulino[h] and Salvatore Petralia*[abei]

Carbon nanodots (CDs) are an emerging class of nanomaterials that have recently attracted significant attention for applications in personalized diagnosis, therapy and theragnostics. Herein, we aimed to develop emissive and photothermal N-doped CDs obtained *via* one-pot thermal process from chitosan (CDs-chit) without the use of organic solvents and additional reagents. The CDs-chit nanostructures were characterized using spectroscopic techniques, including Nuclear Magnetic Resonance (NMR) and Fourier Transform Infrared spectroscopy (FTIR), X-rays Photoelectron spectroscopy (XPS), and Transmission Electron Microscopy (TEM). The CDs-chit showed excellent luminescence quantum yield ($\varphi_{420\,nm}$ = 6%), curcumin entrapment efficiency (12%), good photothermal conversion efficiency upon blue-light excitation ($\eta_{405\,nm}$ = 57.1%) and red-light excitation ($\eta_{808\,nm}$ = 16.2%). The photoxidation and photoreduction properties of CDs-chit nanostructures were also demonstrated through the photodegradation of methylene blue and the photogeneration of gold-nanostructures (CDs-chit/Au^0), a tentative mechanism was proposed whereby CDs-chit act as both electron source and capping agent. *In vitro* experiments using MTT assay demonstrated the low cytotoxicity of CDs-chit. Confocal laser scanning microscopy imaged the cellular uptake of curcumin-loaded car-bon dots (CDs-chit/curc), while the absence of significant changes in gene expression confirmed the biocompatibility of the carbon dots. NIR light-triggered cell damages was observed upon photoexcitation of tumoral HCT 116 cells using an 808 nm laser source through a two-photon absorption mechanism. The ease of preparation, curcumin loading capacity, effective cellular uptake, and downregulation of pro-inflammatory IL-6 gene expression, photoluminescence and hyperthermia make CDs-chit nanomaterials attractive for further investigations in the field of biomedical research.

Received 11th December 2025,
Accepted 1st March 2026

DOI: 10.1039/d5ma01450f

rsc.li/materials-advances

Introduction

Carbon nanodots (CDs) are low-dimensional nanostructures com-posed of an emissive, photothermal and electroactive sp^2-hybridized carbon core, covered by carbonaceous surface terminations such as carboxyl, epoxy, hydroxyl, amide or amine groups, and in some cases even entire precursor molecules. The organic shell of the CDs enables water dispersibility, chemical functionalization, drug loading, low cyto-toxicity, and receptor binding. Over the past decade, considerable interest in CDs has grown due to their facile synthesis,[1] distinctive optical, electronic, and chemical properties.[2–5] Photo-physical properties such as photoluminescence, photo-thermal con-version and photocatalysis are important parameters for a wide range of applications, including bioimaging, light-triggered cancer treatments, photocatalysis and biosensing. Regarding photoluminescence, three main models

[a] *Department of Drug and Health Sciences, University of Catania, 95123 Catania, Italy. E-mail: salvatore.petralia@unict.it*
[b] *CNR-Institute of Biomolecular Chemistry, 95126 Catania, Italy*
[c] *Department of Biomedical and Biotechnological Sciences, University of Catania, 95123 Catania, Italy*
[d] *Faculty of Medicine and Surgery, "Kore" University of Enna, s. Panasia, 94100 Enna, Italy*
[e] *AIDA srl via S. Sofia, 97 Torre Biologica, 95123 Catania, Italy*
[f] *Department of Physics and Astronomy "Ettore Majorana" University of Catania, 95123 Catania, Italy*
[g] *CNR-Institute of Science and Chemical Technologies "Giulio Natta", 20138 Milano, Italy*
[h] *Department of Chemical Sciences, University of Catania, 95123 Catania, Italy*
[i] *NANOMED Research Centre for Nanomedicine and Pharmaceutical Nanotechnology University of Catania – Viale A. Doria 6, 95124 Catania, Italy*
† These authors equally contributed.

have been proposed in the literature to explain the emission mechanism in CDs. The first mechanism, based on the band-gap transition model, assumes that the emission originates from the quantum confinement effect of conjugated π-domains within the carbon core, resulting in an emission wave-length dependent on the core confinement.[6] The second mechanism relies on a surface state emission model, where surface states, resulting from the synergetic hybridization of surface chemical groups and the carbon core, generate traps that induce radiative recombination of excited electron–hole pairs. This mechanism is supported by the observation of dual-emissive bands in the CDs, where the high energy band is attributed to core emission and the low-energy band to surface state emission.[7] Finally, the third mechanism is due to organic fluorophores located either on the surface or within the carbon core, which can produce independent emissions from the molecular surface state or the carbon core state.

Various precursors have been proposed for the synthesis of CDs including citrate, polymers, urea, amino acids, carbohydrates, vitamins, and several natural compounds.[8] Biopolymers constitute an interesting class of materials for use as precursors in the synthesis of CDs, owing to their low cytotoxicity, stability and excellent dispersibility in aqueous media. In this scenario, chitosan is an abundant natural nitrogenous biopolymer obtained from the deacetylation of chitin. It is a copolymer of D-glucosamine and *N*-acetyl-D-glucosamine. Chitosan is soluble in acidic media and its biocompatibility, biodegradability, gelling properties, high nitrogen content, and multiple functional groups (such as acetamido, amino, and hydroxyl groups) make it a valuable precursor for the preparation of N-doped nanomaterials. The most common nanomaterials derived from chitosan include chitosan-nanoparticles,[9] chitosan-microspheres,[10] chitosan-hydrogel[11] and more recently chitosan-CDs.[12] In CDs nanostructures, chitosan acts as both a C and N precursor for the preparation of N-doped CDs. The outstanding properties of chitosan-based nanomaterials have shown great potential in several research areas, such as drug delivery, bioimaging, sensing, gene delivery, and the diagnosis and treatment of various diseases.[13] Many examples of chitosan-derived CDs prepared through different processes such as hydrothermal, microwave, and chemical reactions using additives like citric acid, urea, ethylenediamine, and amino acids are re-ported in the literature. All these methods produce CDs with C/N-core covered by hydroxyl and carboxylic groups, which result from the complete carbonization of the biopolymer. Parra Saldivar *et al.* provided an insightful review on chitosan-based CDs, thoroughly discussing their structural characteristics and properties. The review covers preparation method and explores a broad spectrum of applications spanning biomedicine, environment, and energy.[14]

Here, we report a new one-pot approach based on a mild-thermal process for the preparation of CDs nanostructures composed of a N-doped carbon core covered by a chitosan-derived shell (CDs-chit) (Scheme 1A). Optical properties, including absorption, luminescence, and photothermal effect, were investigated to evaluate the potential of CDs-chit as a semiconductor and

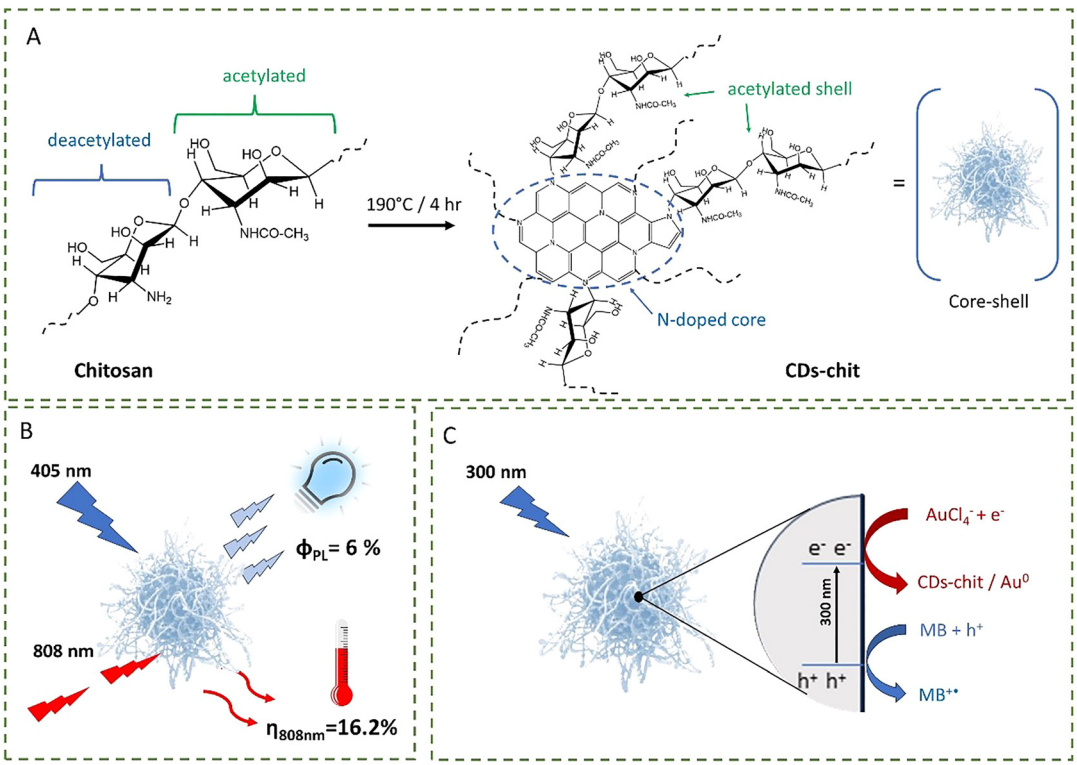

Scheme 1 CDs-chit nanostructures: (A) schematic chemical procedure for the synthesis of CDs-chit nanostructures by thermal treatment of chitosan precursor, (B) photoluminescence and photothermal properties, and (C) photoreduction and photo-oxidation activity.

light-activated material for remotely controlled hyperthermia and imaging (Scheme 1B). Photo-oxidation and photoreduction properties were evaluated by photodegradation of methylene blue and photogeneration of Au-nanostructures upon light photoexcitation at 300 nm (Scheme 1C). The drug loading capacity of CDs-chit was assessed through the preparation of a CDs-chit/curcumin adduct which was studied by spectrophotometry and molecular modelling simulation. Finally, biological experiments demonstrated the low cytotoxicity and effective internalization of CDs-chit/curcumin into human cells, as well as its impact on biochemical pathways through gene expression evaluation.

Results and discussion

Synthesis of N-doped CDs-chitosan (CDs-chit)

We devised tailored CDs-chit, which could have the following characteristics: (i) an inner N-doped carbon core (formed by quaternized N and sp^2 hybridized C) and an outer shell of chitosan-derivatives, (ii) high water dispersibility and biocompatibility, (iii) emissive and photothermal properties, (iv) photoreduction activity and templating and capping effects for the formation of Au nanostructures, (v) photo-oxidation/reduction activity (vi) drug loading capacity, and (v) low cytotoxicity and cell internalization properties. The N-doped CDs-chit were prepared by using a one-step mild-thermal method, recently developed in our laboratories,[15–17] based on the simple heating of chitosan at 190 ± 5 °C in air for 4 hours. The process was carried out without solvents, oxidizing agents and instrumentation currently used for the preparation of carbon nanodots. Fig. 1A illustrates the mechanism proposed for the formation of N-doped CDs based on the Maillard reaction, which is the reaction between an amino group and carbohydrates to produce heterocyclic nitrogen compounds as widely demonstrated in the literature for similar compounds.[18,19] When the chitosan is heated at 190 °C the amino group and aldose group of the chitosan sugar moieties condense to produce N-substituted glycosylamine. The glycosylamine is converted to ketosamine, *via* Amadori rearrangement, which upon dehydration and fragmentation produces aldehydes and aldol groups. Finally, aldehyde-amine condensation generates heterocyclic nitrogen compounds such as pyridines, pyrazines,

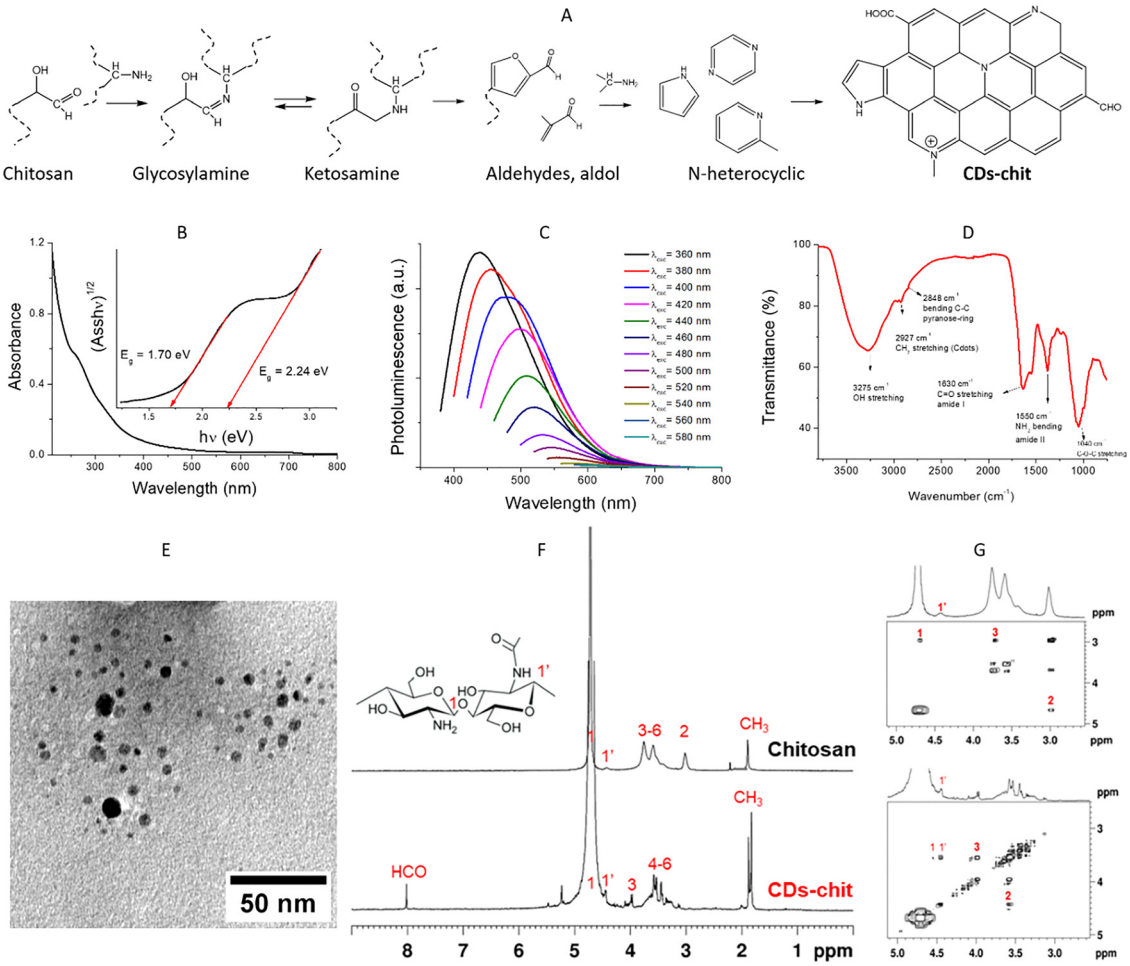

Fig. 1 CDs-chit characterization: (A) proposed mechanism for the formation of CDs-chit N-doped core. (B) Optical absorption spectrum (1 mg mL^{-1}), in-set the Tauc plot for the optical band gaps evaluation. (C) Fluorescence spectrum at various excitation wavelength. (D) ATR-FTIR spectrum. (E) Representative TEM images. (F) ^{1}H-NMR and (G) 2D-COSY NMR (2.5–5.1 ppm region) spectra of chitosan and CDs-chit (2% DCl in D_2O).

and pyrroles, which undergo carbonization to afford nitrogen-doped CDs. The yield of the preparation process was calculated to be about 26%. This mechanism was corroborated by NMR and XPS investigations (see below). In particular, a signal at 8.01 ppm, related to the aldehydic group (HCO), was observed in the proton spectrum of the CDs-chit (Fig. 1F).

The synthesized CDs-chit exhibited the typical absorption bands of carbon-nanodots. In particular, the UV-Vis optical absorption spec-tra showed a band centred at around 265 nm referred to π–π* transition, that originates from sp^2 carbon, and a lower, and a broad band in the range 300–500 nm, related to the n-π* transition generated from C═C, C═N and C═O bonds (Fig. 1B). The optical band gap was calculated by Tauc plot, that showed the variation of $(\mathrm{Ass}\ h\upsilon)^{1/2}$ *versus* $(h\upsilon)$ for CDs-chit (inset Fig. 1B). The optical energy band gaps for the allowed transitions were estimated to be about E_g = 2.24 eV and E_g = 1.70 eV. This was in good agreement with other aromatic N-doped CDs reported in the literature.[20]

Fig. 1C depicts the photoluminescence emission spectrum of CDs-chit from 360 to 580 nm, at various excitation wavelengths. The graph shows the well-known excitation-dependent emission to suggest a photoluminescence mechanism originated by the conju-gated π-domains on the carbon core. The absence of the dual-emissive bands can exclude the surface state emission mechanism. Interestingly, the emission measurements performed at different pH values do not show significant pH-dependent behaviour, to indicate that not enough NH_2 groups are present on the CDs shell for an effective emission quenching *via* charge transfer (Fig. S1). The photoluminescence quantum yield (φ_{PL}) of CDs-chit in water was calculated to be 6%. The effective carbon nanodot formation was well supported by ATR-FTIR spectroscopy (Fig. 1D), showing the diagnostic peaks of chitosan: 3275 cm^{-1} (N–H, amide stretching), 2927 cm^{-1} (C–H, stretching), 2948 cm^{-1} (C–C, bending pyranose ring), 1630 cm^{-1} (C═O stretching, amide I), 1550 cm^{-1} (N–H bending, amide II), 1040 cm^{-1} (C–O–C bridge stretching). The general size and morphology of CDs-chit were investigated by transmission electron microscopy (TEM). Micrographs revealed the presence of tiny spherical core structures, having a median diameter of 3 nm, with a size distribution ranging from 1.1 nm to 10.5 nm (see graphs in Fig. S2) and larger shell of chitosan-residues. Remarkably, nearly 90% of the nanostructures are $<$ 5 nm (Fig. 1E and Fig. S2). The presence of a shell composed of acetylated chitosan residues was corroborated by nuclear magnetic resonance (NMR) spectroscopy. Chitosan precursor is poorly soluble in D_2O, and its NMR spectra are typically acquired in acidic deuterated water.[21] In contrast, CDs-chit displayed excellent water dispersibility at room temperature. The ^1H and 2D-COSY NMR spectra of CDs-chit, in deuterated water, exhibited the characteristic chitosan residue signals, with H1 protons at 4.56 and 4.66 ppm, H2–H6 protons in the 3.30–4.15 ppm range, and CH_3 protons of the acetyl groups at 1.8–2.0 ppm range (Fig. S3). In acidic water (Fig. 1E), the spectra of CDs-chit, compared with the chitosan precursor, revealed downfield shifts of the H2 ($\Delta\delta$ = 0.51 ppm) and H3 ($\Delta\delta$ = 0.21 ppm) signals, consistent with acetylated sugar moieties. This was further supported by the 2D-COSY NMR spectra (Fig. 1F), which showed an increase in the intensity of the CH_3 and H1 signals of the *N*-acetylglucosamine units and a significant decrease of the H1 signal of the glucosamine units in the CDs-chit spectrum.

The electronic structure of the CDs-chit was also investigated by XPS. In detail, Fig. 2A shows the XPS spectrum of CDs-chit in the C 1s binding energy region. A careful deconvolution of the experimental spectrum required five Gaussians at: 284.3 eV due to the Csp^2 species of the CDs structure; 285.0 eV due to the C–C and C–H sp^3 states, 285.5 due to the C–N states of amide groups (due to acetylated fraction), 286.4 eV due to the alcoholic C–OH states, and 288.2 eV due to both –C═O states of the amide, and C(O)–O states of the hemiacetal group.[22] The intensity ratios of the last-mentioned three Gaussians are 1 : 3 : 1. This last observation suggests an increased atomic concentration of the 285.5 eV and 288.2 eV bands with respect to that at 286.4 eV, whose intensity ratio for chitosan was 1 : 4 : 1. Since the present carbon dots were obtained by pyrolysis of chitosan, it emerges that these obtained dots already contain both C–N and –C═O functionalities. Fig. 2B shows the XP spectrum of CDs-chit in the O 1s binding energy region. The spectral fitting of the rather symmetrical XP band required

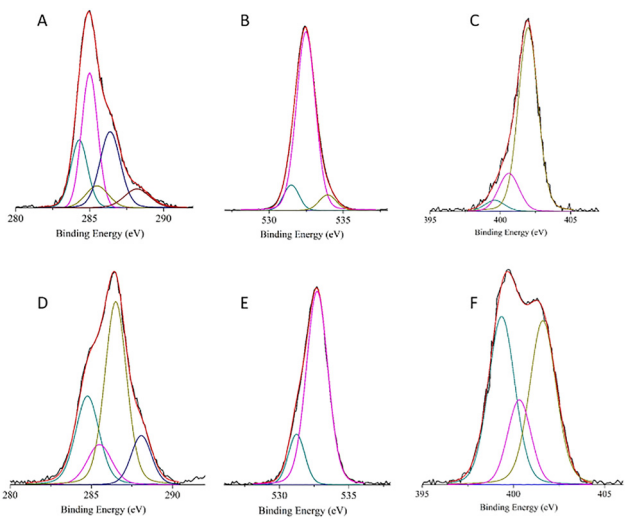

Fig. 2 Al Kα excited XPS spectra of: (A) CDs-chit in the C 1s binding energy region: the dark cyan, magenta, dark yellow, navy, and wine lines refer to the 284.3, 285.0, 285.5, 286.4, and 288.2 eV Gaussians components, respectively; (B) CDs-chit sample in the O 1s binding energy region: the dark cyan, magenta, and dark yellow lines refer to the 531.5, 532.5, and 533.9 eV. Gaussians com-ponents, respectively, (C) CDs-chit in the N 1s binding energy region: the dark cyan, magenta, and dark yellow lines refer to the 399.6, 400.6 and 401.9 eV Gaussians components, respectively; (D) chitosan in the C 1s binding energy region: the dark cyan, magenta, dark yellow and navy lines refer to the 285.0, 285.5, 286.5, and 288.1 eV Gaussians components, respectively; (E) chitosan in the O 1s binding energy region: the dark cyan, and magenta lines refer to the 531.1, and 532.7 eV. Gaussians components, respectively; (F) chitosan in the N 1s binding energy region: the dark cyan, magenta, and dark yellow lines refer to the 399.3, 400.3 and 401.6 eV Gaussians components, respectively. The blue line represents the background, and the red line superimposed to the experimental black profile refers to the sum of the Gaussian components.

three Gaussians at: 531.5 eV due to the oxygen states of the above-mentioned –C═O groups, 532.5 eV attributable to alcoholic C–O– groups, as well as to some oxygen of the Si substrate, and 533.9 eV due to the sizeable presence of water on the sample surface.[23]

Fig. 2C shows the XP spectrum of CDs-chitosan in the N 1s binding energy region. The spectral fitting required three Gaussians at: 399.6 eV due to the chitosan R-NH_2 levels (relative intensity 5%), 400.6 eV due to the -amide N–C═O levels (relative intensity 16%), and 401.9 eV due to quaternized graphitic nitrogen states (relative intensity 79%) that make water soluble the present chitosan-functionalized carbon dots. This latter component is much more abundant than the others and, according to recent literature data, suggests that the present carbon dots are N-doped.[24] For comparison XPS spectra for the precursor have been recorded, in details, Fig. 2D shows the XP spectrum of chitosan in the C 1s binding energy region. A careful deconvolution of the experimental spectrum required four Gaussians at: 285.0 due to the C–C and C–H states, 285.5 eV due to the C–N states of both amine and amide groups (the last of which is due to some partial acetylation), 286.5 eV due to the alcoholic C–OH states, and 288.1 eV due to both C═O states of the amide, and C(O)–O states of the hemiacetal group.[25] The intensity ratios of the last-mentioned three Gaussians are 1 : 4 : 1, as expected based on the chitosan formula. Fig. 2E shows the XP spectrum of chitosan in the O 1s binding energy region. The spectral fitting required two Gaussians at: 531.1 eV due to the C═O states of the acetylated chitosan, and 532.7 eV attributable to the C–O– groups of the chitosan, as well as to some oxygen of the Si substrate.[26] Fig. 2F shows the XP spectrum of chitosan in the N 1s binding energy region. Two experimental peaks at 399.7, and 401.1 eV are evident. The accurate spectral fitting required three Gaussians at: 399.3 eV due to the R-NH_2 levels, 400.3 eV due to the –NH–C═O levels, and 401.6 eV due to some relevant –N^+ states.[27] The presence of quaternized nitrogen is due to the solubilization process of the sample that was carried out in an acetic acid solution. In summary, the XPS data clearly confirm the presence of chitosan-residues on the CDs shell, with quaternized nitrogen improving the water dispersibility of the nanostructures compared to the chitosan precursor.

The presence of a shell of chitosan residues in the here synthesized CDs-chit depends on the temperature used for the carbonization process. As reported in the literature, no residues of acetylated or deacetylated chitosan rings were detected at higher carbonization temperature. In particular, both Stephen and coworker[28] and Zhang and coworkers[29] reported that by a carbonization process at 300 °C for 2 hours, a complete chitosan pyranose ring decomposition occurs and CDs with amino groups on the surface are formed, as confirmed by positive *Z*-potential and FTIR data.[29] Similarly, we obtained fully carbonized CDs when chitosan was heated at 400 °C for 4 hours (Fig. S4 The formation of CDs-chit, featuring a shell of acetylated chitosan residues as depicted in Scheme 1, was confirmed by dynamic light scattering and zeta potential measurements conducted at various pH values (4.35, 5.7, 7.4, and 10.48 units) at 25 °C. In particular, the experiments indicated for an aqueous dispersion of CDs-chit (1 mg mL^{-1}) a slight variation of the hydrodynamic diameter with increasing pH values: 290.5 ± 9.9 nm at pH 4.35, 294.2 ± 15.4 nm at pH 5.7, 330.8 ± 18 nm at pH 7.4, and 353.7 ± 17.3 nm at pH 10.48. According to the absence of NH_2 groups on the shell, negative values of the *Z*-potential were observed for all the pH range investigated (−15.6 ± 0.5 mV at pH 4.35, −16.1 ± 0.9 mV at pH 5.7, −18.4 ± 1.03 mV at pH 7.4, and −21.4 ± 1.3 mV at pH 10.48). (Fig. S5).

Thus, it is plausible that the deacetylated fraction of chitosan (75–85% abundant) is primarily involved in the formation of the N-doped Carbon core, as suggested by XPS data. Conversely, the acetylated fraction of chitosan (15–25% abundant) contributes to the formation of the outer shell, as supported by FTIR spectra, the negative *Z*-potential values even observed at acidic pH, and the acetyl signals detected in the NMR analysis.

Photophysical properties of CDs-chit. Upon light excitation, CDs-chit exhibited interesting photo-physical properties as photothermal effect, photooxidation, and photoreduction properties. To investigate the photothermal properties, an aqueous dispersion of CDs-chit (100 μL, $Abs_{405\,nm}$ = 0.67, 1.0 mg mL^{-1}) was continuously exposed to a 405 nm laser (211 mW power). The temperature changes were monitored by a thermal camera. When the temperature of the system reached the maximum value of about 41 °C (temperature difference = $T_{max} - T_{environment}$ = 15.5 °C), the laser was switched off and the temperature changes during cooling were monitored to confirm the heat transfer of the system (Fig. 3A). A photothermal conversion efficiency (η) value of 57.1% was calculated (Fig. S6). The laser power-dependent behaviour was confirmed by the experiments performed at different

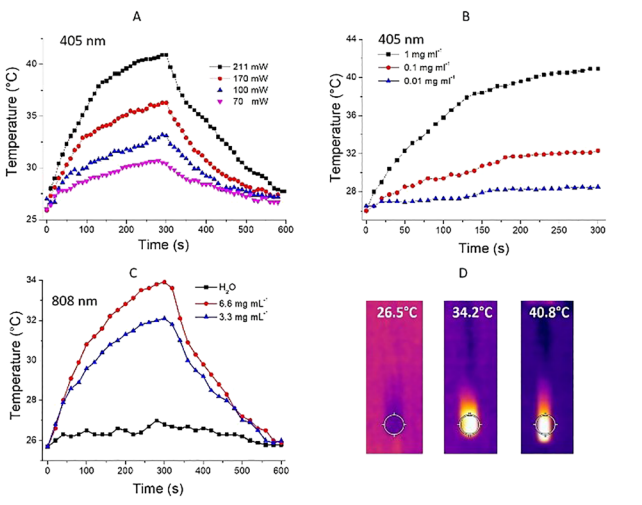

Fig. 3 Photothermal experiments for CDs-chit water dispersion: (A) representative photothermal cycles of CDs-chit (1 mg mL^{-1}, 100 μL) upon photoexcitation with laser 405 nm at different laser power 70, 100, 170 and 211 mW. (B) Photothermal effect of CDs-chit at different amounts of CDs-chit (laser 405 nm power 211 mW). (C) Two-photon photothermal effect of CDs-chit water dispersion (6.6 mg mL^{-1} and 3.3 mg mL^{-1}) upon photoexcitation with NIR-light (808 nm, 1 W) and (D) representative thermograph during the photothermal experiments.

laser powers of 70, 100, 170, and 211 mW, which resulted in corresponding T_{max} values of 30.6, 33.2, 36.2, and 41.0 °C, respectively (Fig. 3A). To better investigate the correlation between the photothermal activity and the amount of CDs-chit, experiments were performed using different amounts of CDs-chit. The results in Fig. 3B show temperature increases of approximately 41.0, 32.2, and 28.4 for CDs-chit concentrations of 1.0, 0.1 and 0.01 mg mL^{-1}, respectively.

A photothermal effect, through the well-known two-photon mechanism,[30] was even observed when the CDs-chit samples were photoexcited by a NIR-light source (808 nm). In particular aqueous dispersions samples of CDs-chit (100 μL, 3.3 mg mL^{-1} and 6.6 mg mL^{-1}), with negligible absorption values above 700 nm, were continuously exposed to 808 nm laser source (1 W power). The increases of temperature upon 5 minutes of photoexcitation, monitored by a thermal camera were 8.2 °C and 6.3 °C for the sample at 6.6 mg mL^{-1} and 3.3 mg mL^{-1}, respectively (Fig. 3C). The photothermal conversion efficiency (η) values of 17.1% (τ_s = 122.9 s) and 15.2% (τ_s = 102.7 s) were calculated for the sample at concentration 6.6 mg mL^{-1} and 3.3 mg mL^{-1} respectively. These data clearly indicate the red-light triggered photothermal property of CDs-chit by two-photon mechanism with an average photothermal yield conversion value of about η = 16.2% (τ_s = 112.8 s). Representative thermographs of the photothermal experiments are depicted in Fig. 3D. The temperature environment during all experiments was about 25.8 ± 0.5 °C.

The optical band gap values calculated by Tau's plot equation (1.7–2.24 eV) suggest the semiconductor properties of CDs-chit, through the photogeneration of reducing-electrons and oxidizing-holes species, as recently reported for similar CDs.[17] In particular, the photoreducing properties of CDs-chit were investigated through the photochemical formation of Au^0 nanostructures. Upon photoexcitation of a CDs-chit water dispersion (1 mg mL^{-1}) containing $HAuCl_4$ (0.56 mM) a rapid formation of gold nanoparticles was observed, evidenced by the emergence of a localized surface plasmon resonance (LSPR) absorption band in the visible region at around 590 nm (Fig. 4A).

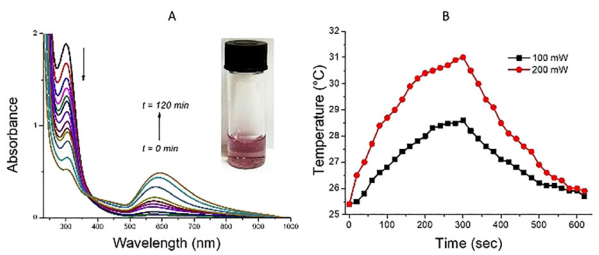

Fig. 4 CDs-Chit/Au nanostructures: (A) changes in the optical absorption spectrum of a CDs-chit water dispersion during the Au-nanostructure photogeneration (CDs-chit 1 mg mL^{-1}, $HAuCl_4$ 0.56 mM, 2 lamps at 300 nm, different times: 0, 2, 4, 6, 8, 10, 15, 20, 25, 30, 45, 75, and 120 min). Inset: photograph of the CDs-chit/Au water dispersion. (B) Photothermal experiments for CDs-chit/Au dispersion in water (100 μL, $A_{532\,nm}$ = 0.176), upon photoexcitation with Laser CW 532 nm at power values 100 and 200 mW.

The disappearance of the Au^{III} band at around 302 nm and the for-mation of the LSPR band at around 580 nm with a net isosbestic point at around 344 nm indicated the direct conversion of Au^{III} to Au^0. The CDs-chit are crucial for the photogeneration of the Au nanostructures. In particular, the carbonaceous core of the CDs-chit nanostructures, by absorbing UV-photons (300–400 nm), produces free-electrons (e^-) and hole (h^+) by the reaction (1), the free-electron induces the photoreduction reaction (2) while the chitosan shell acts as a capping agent determining shape, size and water dispersibility of the photogenerated Au nanostructures.

$$\text{CDs-chit} + h\upsilon\ (300\ \text{nm}) \rightarrow \text{CDs-chit}(h^+) + e^- \quad (1)$$

$$Au^{III}Cl_4^- + 3e^- + n\text{CDs-chit} \rightarrow (\text{CDs-chit})_n/Au^0 + 4Cl^- \quad (2)$$

Control experiments, in which an aqueous dispersion of CDs-chit (1 mg mL^{-1}) and $HAuCl_4$ (0.56 mM) was stirred in the dark for different times, confirmed the photoinduced generation of Au nanostructures. Indeed, in the absence of photoexcitation, no LSPR band appeared in the optical spectra (Fig. S7).

To investigate the photothermal properties of CDs-chit/Au^0, an aqueous dispersion of sample (100 μL, $A_{532\,nm}$ = 0.176) was continuously exposed to a 532 nm laser source. The temperature changes were monitored using a standard thermal-camera. Fig. 3B illustrates the representative photothermal cycles of the nanostructures during photothermal experiments at various laser powers (100 and 200 mW). When the temperature of the system reached the maximum value (T_{max}), the laser was switched off and the tempera-ture dropped to environmental temperature (T_{env}). The power-dependent behaviour was confirmed by experiments performed with different laser powers and the temperature values recorded were approximately 28.6 and 31.1 °C with 100 and 200 mW laser power, respectively (Fig. 4B). The T_{env} was around 25.3 °C. Two representative photothermal cycles for these experiments are reported in Fig. S8. A photothermal conversion efficiency (η) value of about 28.6%, with a photothermal time constant (τ_s) value of about 123.1 s, was calculated by Roper's equation (Fig. S9). Recently, similar nano-hybrid systems have been proposed for biomedical applications including drug delivery,[31] bioimaging,[32] and DNA sensing.[33]

The photooxidant properties of CDs-chit nanostructures were spectroscopically confirmed by using methylene blue (MB) as h^+ scavenger, through the reaction (3).

$$\text{MB} + \text{CDs-chit}(h^+) \rightarrow \text{CDs-chit} + \text{MB}^{+\bullet} \quad (3)$$

The MB will form by-product for standard photodegradation pathway.

Fig. 5A illustrates the optical absorption spectra of the CDs-chit/MB (1 mg mL^{-1}) water dispersion upon UV-light irradiation (300 nm) in deaerated conditions and at different irradiation times (10, 20, 30, 40, 50, and 60 min). The decreases of the MB absorption band at around 665 nm confirmed the rapid photodegradation of MB. The control experiment conducted in aerated condition demonstrated that in the presence of O_2 the

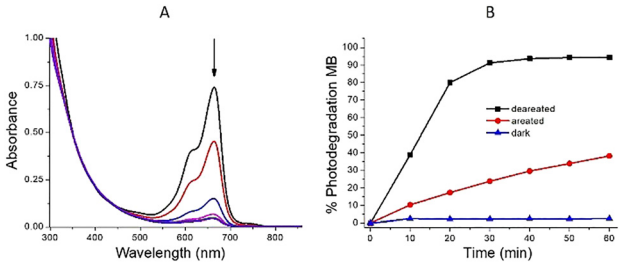

Fig. 5 Photooxidation experiments of CDs-chit (1 mg mL^{-1}) water dispersion in the presence of MB upon UV-light irradiation (10, 20, 30, 40, 50, and 60 min, 2 lamps 300 nm): (A) optical absorption spectra in the region 300–850 nm of CDs-chit/MB dispersion and (B) MB photodegradation (%) in aerated, deaerated and dark conditions.

MB photodegradation does not occur (Figure S10) due to the photo-quenching of O_2.

The photoinduced oxidation was also confirmed by the experiments conducted in dark conditions. In this case no MB photodegradation was observed (Fig. S11). Fig. 5B summarizes the MB photodegradation (%) in aerated, deaerated and dark conditions. It is known that upon photoexcitation with UV-photons (300 nm) in the absence of oxygen the reaction (3) is dominant.

Biological experiments

Cytotoxicity experiments. To assess the effect of CDs-chit on cell viability, MTT assays were performed on human colorectal adeno-carcinoma cells (CaCo-2). In details, an amount of 5000 cells was exposed to increasing amounts of CDs-chit (0.04, 0.4, 4.0, and 40 μg) for 24 hours as reported in the experimental section. As illustrated in Fig. 6, a reduction of the cell viability of only 3.25% (p-value: 0.6673) and 0.25% (p-value: 0.9996), compared with the untreated control, was observed for the cells treated with 0.4 and 0.04 μg of CDs-chit, respectively. No remarkable effect on cell morphology was observed. At higher concentrations of CDs-chit, 4 μg and 40 μg, cell mortality of 23.2% (p-value: <0.001) and 37% (p-value: <0.001) were recorded, respectively. The results clearly show a dose-dependent effect of CDs-chit on the cell viability. At the lowest concentrations (0.04 and 0.4 μg), the CDs-chit are well tolerated by the cells, suggesting a low level of initial cytotoxicity.

Curcumin loaded CDs-chit nanostructures: preparation and characterization. To ascertain the drug loading capability of CDs-chit, curcumin (curc), a poorly water-soluble natural drug, was loaded in the CDs-chit nanostructures. To prepare the supramolecular adduct (CDs-chit/curc) an excess of curc (1 : 3, w/w) was added to a CDs-chit dispersion and the mixture was stirred for 72 hours in the dark. Then, the sample was centrifuged (13 000 rpm, 10 min) to remove the unentrapped drug. The formation of the CDs-chit/curc adduct on PBS was confirmed by spectroscopic method.

The UV-vis absorption spectrum of CDs-chit/curc (Fig. 7A) showed the typical curcumin absorption band in the range 400–480 nm and the typical π–π* band of the CDs at around 265 nm. The curcumin loading capacity, calculated as reported in experimental section, was found to be about 3.5% while the entrapment efficiency was calculated to be about 13%.

Molecular Modelling simulations were employed to investigate the geometry of the CDs-chit/curc adduct, which was optimized using the Compass Force Field. In details, ten structures were selected and further subjected to optimization at the DFT level. After simulation investigations, three lowest-energy geometries named G1, G2, and G3 were obtained (Fig. 7B). The energy of structure G1 was considered as reference (E = 0.00 kcal mol^{-1}), while the energy of the G2 and G3 were calculated to be +13.24 kcal mol^{-1} and +16.95, respectively. The lowest-energy structure (G1) is characterized by three electrostatic interactions between the curcumin molecule (exposing the enolic group and the two phenolic oxygens) and three amide groups present in the CDs-chit shell. These long-range electrostatic interactions stabilize the aggregation curcumin-chitosan more effectively than the van der Waals interactions for the G2 and G3 structures. The simulated UV-Vis spectrum corresponding to structure G1 is shown in Fig. S12. The simulated spectrum exhibits an absorption peak in the range 380–482 nm, attributed to the π–π* electronic transition for curcumin, consistent with the one observed in the experimental spectrum at 400–480 nm (Fig. 5A), at lower wavelength the absorption of the chitosan acetyl group was also recorded.[34]

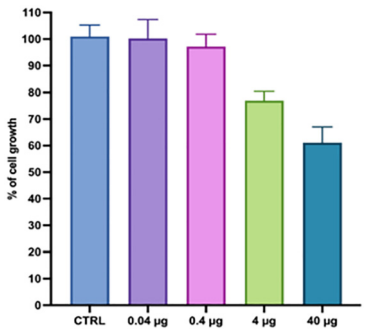

Fig. 6 Viability of human colorectal cells treated for 24 hours with increasing concentrations of CDs-chit (0.04, 0.4, 4.0, and 40.0 μg). Bars are means SEM of three independent experiments with n = 3.

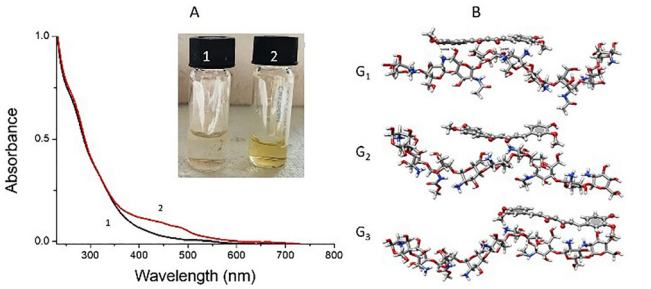

Fig. 7 CDs-chit/curc: (A) UV-Vis optical absorption spectra of CDs-chit (line 1) and CDs-chit/curc (line 2), insets photographs of CDs-chit (1) and CDs-chit/curc (2). (B) CDs-chit/curc geometries: G1, G2 and G3. Minimum geometries of different structures after DFT calculation at B97D/6-311+G(d,p)/CPCM level.

The spectroscopically data clearly indicated an enhancement of the curcumin solubility (Fig. 7A red-line 2) due to the CDs-chit/curc complex formation. This complex formation is corroborated by the modelling simulation results indicating effective electrostatic interactions between the curcumin and the amide termination in the outer CDs-chit shell, as well as the simulation absorption in the curcumin range absorption.

RNAseq experiments. In order to investigate the effect of the CDs-chit/curc adduct on metabolic pathway of human cells, the gene expression of 48 genes of HeLa and HTC-116 cells treated with the nanostructures were investigated by RNAseq assay.[35] The results showed for the treated HeLa cells no statistically significant differences with the untreated control for all the genes investigated (Fig. 9), to indicate an excellent metabolic biocompatibility. Similarly, the experiments performed for the HCT-116 cell line showed no statistically significant differences for all genes except the IL-6 gene, which showed a significant gene expression downregulation (Log2 Fold Change = −6.18 *p*-value = 0.01) (Fig. 8).

The observed down regulation of IL-6 (a pro-inflammatory cytokine often implicated in tumor progression and immune evasion)[36] is indicative of the CDs-chit/curc anti-inflammatory activity, which could promote the inflammation-driven reduction of the tumor pro-liferation[37] and sensitizing to immune-mediated attacks.[38] These data clearly suggest the good biocompatibility of the CDs-chit/curc nanostructures with both cell lines investigated. The un-changed gene expression observed clearly indicates that CDs-chit/curc do not affect the transcriptional homeostasis, a key factor to ensure protection in non-cancerous cells. All numerical data on fold change are reported in Tables S3 and S4. Further studies should aim to investigate the biochemical pathways modulated by CDs-chit/curc in different human tissues.

Cellular internalization experiments. Confocal imaging experiments were performed to evaluate the potential of CDs-chit/curc as a drug delivery system. Fig. 9 illustrates representative bright-field (9A) and confocal fluorescence (9B) images of HeLa cells at different conditions: untreated and treated cells with CDs-chit/curc adduct (4.0 μg μL^{-1} and 40 μg μL^{-1}). Untreated cells (control = CTRL) showed no significant emission apart slight cell auto-fluorescence (10.2 ± 1.5 u.a). Compared to the control, a net in-crease in fluorescence signal of 14.6 ± 1.9 u.a and 63.3 ± 7.7 u.a was recorded for the cells treated with 4 μg μL^{-1} and 40 μg μL^{-1} of CDs-chit/curc, respectively. This finding evidenced the effective internalization of CDs-chit/curc adducts in the cytoplasm (Fig. 9C).

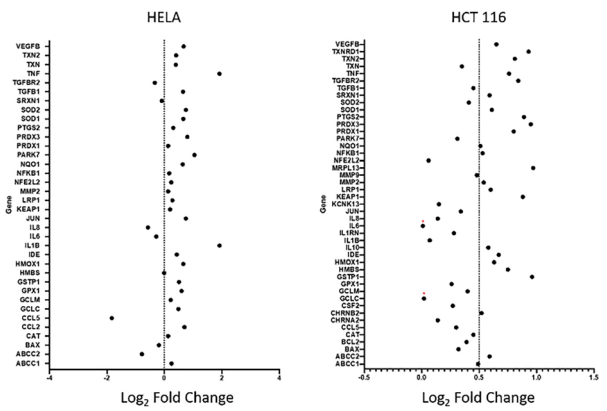

Fig. 8 Gene expression difference, calculated as log2 (fold change), in HeLa cells and in HCT-116 cells treated with CDs-chit/curc compared to control. $p \leq 0.001$: *** (highly significant), $0.001 < p \leq 0.01$: ** (significant), $0.01 < p \leq 0.05$: * (moderately significant), $p > 0.05$: ns (not significant).

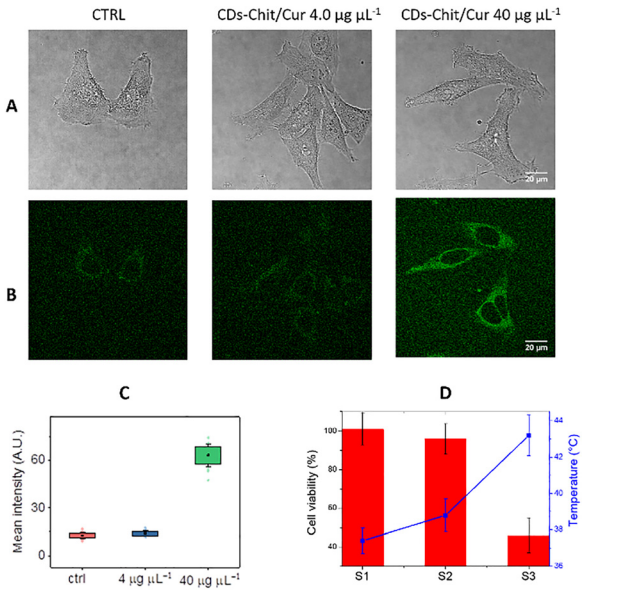

Fig. 9 CDs-chit/curc cell internalization experiments: (A) representative bright-field and (B)confocal fluorescence images of HeLa cells not exposed to CDs-chit/curc nanoparticles (ctrl) and after incubation with different amounts of CDs-chit/curc adduct (4.0 μg μL^{-1}). (C) Average fluorescence intensity, reflecting the intracellular uptake of the nanostructures at increasing concentrations. (D) NIR-triggered cell damages of CDs-chit/curc on HCT-116 cells upon photoexcitation with NIR-laser 808 nm; 1 W: MTT analysis of the not irradiated cells treated with nanostructures (S1), irradiated untreated cells (S2) and cells treated with nanostructures and irradiated (S3).

Proof-of-concept of *in-vitro* light-triggered cancer cell damage experiments. Due to the peculiar photophysical properties of CDs-chit, photo-excitation of nanostructures with red-light could result in cell mortality through the light-to-heat conversion. To evaluate the light-triggered cancer cell damage, HCT-116 cells in the presence of 3.3 mg mL^{-1} of CDs-chit/curc were irradiated by a CW laser 808 nm for 15 min. The temperature of each sample during the experiments was monitored by a thermal-camera, recording a value of 37.4 ± 0.7 °C for the not irradiated cells treated with CDs-chit/curc (S1), 38.8 ± 0.9 °C for the irradiated cells without CDs-chit/curc (S2) and 43.2 ± 1.1 °C for the irradiated cells treated with CDs-chit nanostructures (S3). The cell viability for all samples was investigated, by a standard MTT test after 24 h of incubation, showing no significant effect on the cell viability of the not irradiated samples (S1) and the irradiated cells without CDs-chit (S2), while an effective cytotoxic effect was evident on the irradiated cancer cells treated with CDs-chit and exposed to

Table 1 Comparison of CDs-chit prepared by different synthetic approaches

Preparation methods	PL-Q.Y. (%)	Emission λ (nm)	Absorption λ (nm)	Cells viability (%) cell lines (amount of CDs)	LC-EE (%) (drug)	Photothermal η (%)	Size (nm)	Ref.
Microwave	—	310–400	280	—	—	—	0.6–8.7	39
Hydrothermal	—	462	231–330	100%, L929 (2–50 μg mL^{-1})	—	—	4 ± 1	40
Carbonization 200 °C/10 h	—	468–554	300–600	—	—	—	2.7 ± 0.5	41
Carbonization 300 °C/2 h	4.34%	365	261	>85%, L929 (2–200 μg mL^{-1})	—	—	1–6	42
Hydrothermal acid 80 °C/30 min	—	400–415	260	(97%, IC-21 and SH-SY5Y (10–100 μg mL^{-1})	EE: 32% (Dopamine)	—	2.7	43
Carbonization 300 °C/2 h	—		300	—	—	Discussed but not declared	—	44
Autoclave Acid 180 °C/2 h	35%	400 (Exc. 330 nm)	230–290	93%, *E. Coli* and *B. subtilis* (20–400 μg mL^{-1})	—	—	2.8 (*via* HRTEM)	45
Chitosan loaded on preformed CDs	20%	450	360	88% viability on HeLa cells (4–32 μg mL^{-1} Cds-chit)	EE: 60.4% (Doxorub.)	—	85	46
	—	345	280–350		—	—	2.34–5.88	47
	—	432	282	—	—	—	—	48
Carbonization 190 °C/4 h	6%	430–480	265 nm, 300–500 nm	96.75–73%, CaCo-2 (1–100 μg mL^{-1})	LC: 3.5% EE: 12% (Curcumin)	57.10% (405 nm), 15% (808 nm)	1.1–10.5	This work

Note: LC = drug Loading Capacity, EE = Entrapment Efficiency, PL-Q.Y. = Photoluminescence - Quantum Yield, η = photothermal yield conversion.

red-light (S3) with a cell mortality of about 57.8 ± 1.1%. (Fig. 9D). This data suggests a potential red-light photothermal cells damaged induced by CDs-chit nanostructures through a two-photon mechanism. Further investigations will be performed using different cells lines and various CDs-chit amount.

To assess the stability of CDs-chit nanostructures optical absorption spectra of lyophilized samples dissolved in deionized water were recorded after 2 weeks, 1, 3 and 6 months from preparation. No significative spectra variation was observed overtime for all samples investigated to suggest the good stability of the nanosystem (Fig. S14). Furthermore, the drug loading capacity of the CDs-chit-curcumin was measured after six months of the preparation, obtaining a DL% value of about 3.1%, comparable with the DL% value of 3.5% obtained for the fresh prepared CDs-chit. In addition, no significative spectra changes were observed in PBS after 6 months from the preparation for CDs-chit/Curc complex (Fig. S15). All these data indicate a good stability of the CDs-chit system overtime. Moreover, the straightforward chemical and photophysical properties of CDs-chit such as high water dispersibility, good stability, excellent light-to-heat photothermal conversion, photoluminescence, photoreduction-oxidation properties together with drug loading capacity and low cytotoxicity makes the proposed chitosan-based nanostructures an appealing system for photothermal/photodynamic therapies, cell's tracking and drug delivery process.

Literature overview. The Table 1 provides a direct comparison of the optical properties (quantum yield emission, photothermal conversion yield), size, morphology, cytotoxicity, cell's internalization and drug loading efficiency for CDs-chit prepared *via* a single-pot approach using microwave, hydrothermal, and carbonization methods,[39–45] and by functionalization of preformed CDs with chitosan.[46–48] All nanostructures exhibit good blue-green luminescence, small size (<10 nm) and low cytotoxicity. To the best of our knowledge, this work is the most complete report to describe the properties of chitosan-based nanostructure prepared using an unprecedented thermal approach. Moreover, the investigation of tumour cell uptake and drug loading capacity together with the emission and NIR-triggered photothermal effect of CDs-chit have never been reported in the literature.

Conclusions

Luminescent and red-triggered photothermal chitosan-derived nitrogen-doped carbondots (CDs-chit) were synthesized *via* thermal processing of chitosan precursor. A structure composed of a N/C core capped with chitosan-derived acetylated moieties was proposed and confirmed through various characterization techniques. The resulting bioinspired photo-responsive CDs-chit nanostructures showed excellent water dispersibility, spherical morphology, and nanometer size. Their emissive behaviour, as well as light-triggered photothermal, photoxidizing, and photoreducing properties were also demonstrated. Under light irradiation, CDs-chit promoted the formation of photothermal gold nanoparticles stabilized by the carbon nanostructures. CDs-chit exhibited low cytotoxicity in human cells and the ability to load curcumin (CDs-chit/cur), selected as a model of a poorly water-soluble drug. Molecular modelling simulations provided insights into nanocarrier-drug interactions. Confocal laser scanning microscopy confirmed cellular uptake of CDs-chit/cur while RNA-seq revealed no significant alterations in metabolic pathways. In particular, no changes were detected in the expression of the 48 genes examined, except for a downregulation of IL-6 gene expression in HCT-116 cells, consistent with the known anti-inflammatory activity of curcumin. Photothermal-induced cellular damage was demonstrated upon NIR-light irradiation using an 808 nm laser source. The bio-friendly preparation, conducted without organic solvents or reagents, combined with favourable

physicochemical properties, hyperthermia, biocompatibility, tumour cell uptake, and drug loading capacity are characteristics that make CDs-chit an appealing candidate for combined chemo-photothermal cancer therapy.

Materials and methods

Chemicals

All chemicals were obtained from commercial sources in the highest possible purity and were used as received. Milli-Q-grade water was used in all preparations. The ultra-filtration devices were Amicon Ultra devices with a 3000 MWCO (3 kDa) cutoff.

Instrumentation

Optical absorption UV-vis spectra were acquired on a PerkinElmer 365 spectrophotometer. A quartz cuvette with an optical length of 10 mm was used. Photoluminescence (PL) spectra were obtained using a HORIBA spectrofluorometer. The emission was recorded at 90° to the direction of the exciting light with 3 nm slits. The photoluminescence quantum yield (ϕ_{PL}) of the CDs-chit dispersion in water (n = 1.33) was obtained using a solution of quinine sulfate (n = 1.36) as standard (ϕ_{PL} = 0.55). ^{1}H NMR (400.13 MHz) and 2D-COSY NMR spectra were acquired on a Bruker Avance 400^{TM} spectrometer at 297 K. Chemical shifts (δ, ppm) are relative to the residual solvent peak (D_2O, 4.72 ppm). Dynamic light scattering measurements were performed on a ZetaSizer NanoZS90 Malvern Instrument (U.K.), equipped with a 633 nm laser, at a scattering angle of 90° and 25 °C. The size of the particles was calculated from the diffusion coefficient by using the Stokes–Einstein equation. The transmission electronic microscopy (TEM) specimens were prepared by dropping the water suspension of the CDs-chi onto an ultrathin carbon film supported copper TEM grid. The grid was dried overnight at room temperature and inserted in the TEM column of a ZEISS LIBRA200FE microscope for morphological analysis. We calculated the size distribution by measuring the nanoparticles' diameter spanning over the grids to obtain robust statistical data.

Photothermal measurements

The photothermal properties of CDs-chit were investigated by irradiating a glass tube (diameter 3 mm) containing various amounts of CDs-chit dispersion. A volume of 100 μL of the CDs-chit dispersion was irradiated with CW laser 405 nm (different laser power) for various minutes. We used a FLIR infrared thermal imaging camera to measure the temperature of the solution every 20 s, during the heating and cooling processes. Photothermal conversion yield (η%) was calculated using the Rope's equation as described in SI.

Synthesis of CDs-chit

An amount of 200 mg of chitosan (low molecular weight) was pyrolyzed at 190 °C in air for 4 hours. The obtained reddish solid product was dispersed in 2 mL of deionized water by ultrasonic process for 5 min. The unwanted solid aggregates and the excess of the insoluble chitosan were removed by centrifugation (13 000 rpm for 5 min) and then by filtration (pore-size 0.2 μm). Finally, the resulting reddish transparent solution was dialyzed using MilliQ-water through a dialysis membrane (Spectra-Por Float-A-Lyzer G2 black, 3 mL, 3–5 kDa) for 46 hours in deionized water. The obtained CDs-chit were lyophilized and stored at room temperature before the use.

X-ray photoelectron (XPS)

XPS spectra were measured at a 45° take-off angle relative to the surface sample holder, with a PHI 5000 Versa Probe II system (ULVAC-PHI, INC., base pressure of the main chamber 1 × 10^{-8} Pa).[49] Samples, deposited on Si substrates, were excited with the monochromatized Al Kα X-ray radiation using a pass energy of 5.85 eV. The instrumental energy resolution was ≤ 0.5 eV. The XPS peak intensities were obtained after Shirley's background removal.[1,2] Spectra calibration was achieved by fixing the Ag $3d_{5/2}$ peak of a clean sample at 368.3 eV.[50] The atomic concentration analysis was performed by considering the relevant atomic sensitivity factors. The fitting of some XP spectra was carried out, using the XPSPEAK4.1 software, by fitting the spectral profiles with Gaussian envelopes, after subtraction of the background. This process involves data refinement, based on the method of the least squares fitting, carried out until there is the highest possible correlation between the experimental spectrum and the theoretical profile. The residual or agreement factor R, defined by $R = [\Sigma(F_{obs} - F_{calc})^2/\Sigma(F_{obs})^2]^{1/2}$, after minimization of the function $\Sigma(F_{obs} - F_{calc})^2$, converged to the value of 0.03.

Photo-oxidation experiments

An aliquot of CDs-chit (2 mL, 1 mg mL^{-1}) was mixed with methylene blue solution ($Abs_{665\,nm}$ = 0.7398) and irradiated under stirring with 2 lamps (300 nm, 16W). The experiments were replicated three times in both aerated and deaerated conditions (15 min with argon gas) in the dark. The optical absorption spectra were recorded at different irradiation times (10, 20, 30, 40, 50, and 60 min).

Photoreduction experiments (Au-nanostructures formation)

To aliquots of 2 mL of CDs-chit (1 mg mL^{-1}) in water was added a volume of 20 μL of $HAuCl_4$ (1.6 × 10^{-2} M). After degassing in argon for 15 min the sample was irradiated in a photoreactor equipped with 2 lamps (300 nm, 16 W) for 120 minutes. The formation of Au-nanostructures was investigated and confirmed by optical absorption UV-Vis spectra.

Preparation of CDs-Chit/Cur

An excess of solid curcumin (3 mg mL^{-1}) was added to a water dispersion of dialyzed CDs-chit passed through a 0.2 μm GHP filter (20 mg in 2 mL). The mixture was stirred at room temperature for 3 days and in the dark. Then, it was centrifuged at 10 000 rpm for 15 min to give a clear yellow colloidal solution. As a control, curcumin alone was subjected to the same treatment. The amount of curcumin entrapped in the carbon-dots was measured by the optical absorption at 433 nm

in water (ε = 55 000 L mol^{-1} cm^{-1}). Drug loading capacity (LC %) and entrapment efficiency (EE%) were calculated by the following equations:

$$\mathrm{LC}\,(\%) = \frac{\text{mg drug in}}{\text{mg drug in} + \text{mg CDs-chit}} \times 100$$

$$\mathrm{EE}(\%) = \frac{\text{mg drug in}}{\text{mg drug used in formulation}} \times 100$$

Molecular dynamics simulation

The computational models adopted in this study involved positioning a curcumin molecule onto a chitosan polymer. The chitosan structure was modeled by replicating the base polysaccharide sequence of D-glucosamine and *N*-acetyl-D-glucosamine units four times. Only two acetylated groups were retained, while the remaining –NH_2 groups were treated as protonated. The curcumin molecule was modeled in its monoanion-enol tautomeric form.[51] Multiple initial configurations were examined and the resulting complexes were placed in a simulation box with dimensions of 4.5 × 1.5 × 2 nm, solvated with explicit water molecules, and equilibrated through a multi-step procedure (Fig. S13). This process began with 10 000 steps of energy minimization using the steepest descent algorithm and the Compass Force Field, followed by 10 ns molecular dynamics (MD) simulations.[52] Subsequently, an additional 90 ns of MD simulations were conducted, and 10 representative structures were randomly sampled from the last 5 ns. These structures were further refined using density functional theory (DFT) optimization. All MD simulations were conducted at 298 K under periodic boundary condition in NPT ensemble. Pressure was maintained at 1 atm using a Berendsen barostat. A time step of 1 fs was employed to integrate the equation of motion, and long-range electrostatic interactions were calculated using the Ewald summation method. Na^+ and Cl^- ions were added as counterions to ensure overall electric neutrality of the system. For these optimizations, the B97D functional, which incorporates dispersion corrections,[53] was employed in conjunction with the 6-311+G(d,p) basis set. Solvation effects were accounted for using the Conductor-like Polarizable Continuum Model (CPCM).[54] UV–visible absorption spectra were calculated using the time-dependent DFT (TD-DFT) method with the CAM-B3LYP functional[55] and the 6-311+G(d,p) basis set. All quantum mechanical calculations were performed with Gaussian 16 software, while molecular dynamics simulations were carried out using the Discover module within the Biovia Material Studio 2017 package.

Cells growth conditions

Human colorectal adenocarcinoma cells (CaCo-2 HTB-37TM, American Type Culture Collection, Manassas, VA, USA), HeLa-CCL-2 and HCT 116 CCL-247 cells (American Type Cell Culture,Manassas, 10801 University Blvd, United States) have been grown following the standard protocols provided by the ATCC, in DMEM for CaCo-2 (Cat. No. 11965092, Thermo Fisher Scientific, 168 Third Avenue. Waltham 02451, United States) in MEM for HeLa (Cat. No. 41090036, Thermo Fisher Scientific, 168 Third Avenue. Waltham 02451, United States) and McCoy medium for HCT-116 (Cat. No. 16600082, Thermo Fisher Scientific, 168 Third Avenue. Waltham 02451, United States) both with 10% heat-inactivated fetal bovine serum, 2 mM L-Alanyl-L-Glutamine, penicillin–streptomycin (50 units-50 μg mL^{-1}); both cells were incubated at 37 °C in a humidified atmosphere of 5% CO_2, 95% air.

MTT assay

Four serial dilutions of CDs-chit were created: 10 μg μL^{-1}, 1 μg μL^{-1}, 100 ng μL^{-1}, 10 ng μL^{-1} and 1 ng μL^{-1}. CaCo-2 HTB-37TM cells were treated with 40 μL of each solution. Untreated cells were used as controls. Microplates were incubated at 37 °C in a humidified atmosphere of 5% CO_2, 95% air for 24 h, and then cytotoxicity was measured with colorimetric assay based on the use of tetrazolium salt MTT (3-(4,5-dimethylthiazol-2-yl)-2,5-diphenyl tetrazolium bromide. IC_{50}: this parameter expresses the concentration of the tested compound necessary to kill half of the cell population after 24 h of incubation relative to untreated controls. The results were read on a multiwells scanning spectrophotometer (BioTek Synergy H1 Multimode Reader Agilent Technologies, Santa Clara, CA, USA), using a wavelength of 569 nm. Each value was an average of 4 wells.

Confocal microscopy analysis of cellular uptake

HeLa cells were plated (20 000 cells per well) on chambered coverslips (μ-Slide 18 Well Glass Bottom, Ibidi, Gräfelfing, Germany) and allowed to grow overnight. The following day, cells were incubated with different concentration of CDs-chit/Curc (4 μg μL^{-1} and 40 μg μL^{-1}) for 1 hour. After incubation, cells were washed with 1X PBS. Confocal fluorescence images were acquired on a Leica SP8 confocal laser scanning microscope (Leica Microsystems, Wetzlar, Germany) with a 1.4 NA 63 X oil immersion objective (HCPL APO CS2). The microscope has an incubation chamber to keep the cells at 37 °C and 5% CO_2. The pinhole size was set to 1 Airy Unit. 1024 × 1024 pixel images were acquired using a line frequency of 700 Hz with 4-line average with a pixel size of 140 nm. An excitation wavelength of 405 nm was used, and the emission was detected in the band 500–600 nm *via* a hybrid detector, operating in standard mode. The transmitted light detector channel was used to generate a brightfield image and visualize the morphology of the cells. The fluorescence intensity was evaluated by selecting regions of interest (ROI) corresponding to single cells and extracting the average intensity value in the ROI.

Amplicon RNAseq treatments

HeLa and HCT 116 cells were plated in a 6-well plate (Cat. No. 30006, SPL Life Sciences Co., Ltd. 48, Geumgang-ro 2047 beon-gil, Naechon-Myeon, Pocheon-si, Gyeonggi-do 487 835, Korea) at a concentration of 100 000 cell per well and after 24 hours, they were treated for 6 hours with a concentration of CDs-Chit/Cur equal to 40 ng μL^{-1}, that in a working volume of 500 μL

corresponds to 20 μg per well. Each treatment was carried out in triplicate. Untreated cells were used as a control. After 6 hours, cells supernatant was removed and cells were resuspended in 300 μL of RLT Buffer (Cat. 74104, Qiagen, Hilden, Germany) with a concentration of β-mercaptoethanol (Cat. M6250, Merck, 126 East Lincoln Avenue P.O. Box 2000. Rahway 07065, United States) equal to 10 μL mL^{-1} and in 300 μL of 70% ethanol. The cells were finally frozen at −80 °C awaiting RNA extraction.

RNA extraction and quantification

The RNA was extracted following the manufacturer's instructions of the Qiamp RNeasy Mini Kit (Cat. 74104, Qiagen, Hilden, Germany); the integrity and the quantification of the RNA were attest using Agilent RNA 6000 Nano Kit (Cat. 5067-1511, Agilent, Santa Clara, CA 95051, USA) on a 2100 Bioanalyzer Instrument (Cat. G2939BA, Agilent, Santa Clara, CA 95051, USA) and also using Qubit TM RNA HS Assay Kit (Cat. 2390601, Invitrogen, Eugene, Oregon, USA) on a Qubit 4 Fluorometer instrument (Cat. Q33238, Invitrogen, Eugene, Oregon, USA). The samples and their quantifications are given in Table S1.

Amplicon RNAseq libraries preparation and sequencing

The libraries have been prepared following the manufacturer's instructions provided by the protocol generated by the website https://support.illumina.com/custom-protocol-selector.html and specifying the following supported combinations (Table S2). The RNA input used was 100 ng for all samples. The preparation was carried out by the AmpliSeq TM cDNA Synthesis for Illumina kit (Cat. 20022654, Illumina Inc., San Diego, California, USA) for retrotranscription, the AmpliSeq TM Library PLUS for Illumina (Cat. 20019102, Illumina® Inc., San Diego, California, USA) for preparation and the AmpliSeq TM CD Indexes, Set A for Illumina® (96 Indexes, 96 Samples) (Cat. 20019105, Illumina® Inc., San Diego, California, USA) for sample indexing. The denaturing and dilution of libraries were performed following the ''Denature and Dilute Libraries Guide'' protocol provided by Illumina® (Document # 15039740 v10). Finally, sequencing was performed using the MiSeq Reagent Kits v3 (Cat. 15043895, Illumina® Inc., San Diego, California, USA) on a MiSeq Instrument (Cat. SY-410-1003, Illumina® Inc., San Diego, California, USA). Bioinformatic analysis, Different Expression Gene and Statistical Analysis were carried out using QIAGEN CLC Genomics Workbench (Qiagen, Hilden, Germany).

CDs-chit/curc cytotoxicity under NIR-light irradiation

To test the effect of light irradiation on the activity of CDs-chit/curc, the HCT 116 cells (5×10^4 cells per well) were incubated in 96-multiwell plates with 3.3 mg mL^{-1} amount of Cds-chit/curc, and exposed to NIR light. Before the experiment, the cells were washed twice with phosphate-buffered saline (PBS), and the medium was replaced with freshly prepared DMEM buffer. The samples were passed through 0.22 μm filters to remove contaminations. Each well was individually exposed for 8 min to light irradiation (λ = 808 nm, 1 W). A treated but nonirradiated wells were taken under the same condition and used as controls. To reduce cellular stress, during light treatment, all samples were taken at 37 °C. During light irradiation, the overheating of the well was monitored by a thermal camera. After photoexcitation, both treated and untreated samples were placed in the incubator at 37 °C and 5% CO_2. After 24 h, the standard MTT test was performed to evaluate the cytotoxicity.

Author contributions

Ludovica Maugeri: investigation, Grazia Maria Letizia Consoli: investigation and writing, Giuseppe Forte: investigation, Giorgia Fangano: investigation, Loredana Ferreri: investigation, Giuseppe Granata: investigation, Paolo Giuseppe Bonacci: investigation, Nicolo Musso: investigation, Luca Lanzanò: investigation, Elisa Longo: investigation, Marcello Marelli: investigation, Angelo Ferlazzo: investigation, Antonino Gulino: investigation, and Salvatore Petralia: writing – review & editing, writing – original draft, visualization, validation, supervision, methodology, investigation, funding acquisition, data curation, conceptualization.

Conflicts of interest

There are no conflicts to declare

Data availability

The data supporting this article have been included as part of the supplementary information (SI). Supplementary information: additional emission and absorption optical spectra, TEM micrographs, NMR spectra, photothermal data, simulated geometry, XPS data, stability test, and fold change data for cell lines. See DOI: https://doi.org/10.1039/d5ma01450f.

Acknowledgements

This work has been funded by Linea di Intervento 1- Progetti di Ricerca Collaborativa del ''PIAno di inCEntivi per la RIcerca di Ateneo 2024/2026''. Project Title: Mhy-Nano. The authors would like to also thank the BRIT laboratory at the University of Catania (Italy) for the valuable technical assistance and use of their laboratories.

References

1 H. Liu, X. Zhong, Q. Pan, Y. Zhang, W. Deng, G. Zou, H. Hou and X. Ji, A review of carbon dots in synthesis strategy, *Coord. Chem. Rev.*, 2024, **498**, 215468, DOI: 10.1016/j.ccr.2023.215468.

2 H. F. Etefa, A. A. Tessema and F. B. Dejene, Carbon Dots for Future Prospects: Synthesis, Characterizations and Recent Applications: A Review (2019–2023), *C*, 2024, **10**, 60, DOI: 10.3390/c10030060.

3 J. Ren, H. Opoku, S. Tang, L. Edman and J. Wang, Carbon Dots: A Review with Focus on Sustainability, *Adv. Sci.*, 2024, **11**, 2405472, DOI: 10.1002/advs.202405472.
4 L. Cui, X. Ren, M. Sun, H. Liu and L. Xia, Carbon Dots: Synthesis, Properties and Applications, *Nanomaterials*, 2021, **11**, 3419, DOI: 10.3390/nano11123419.
5 D. Ozyurt, M. Al Kobaisi, R. K. Hocking and B. Fox, Properties, synthesis, and applications of carbon dots: A review, *Carbon Trends*, 2023, **12**, 100276, DOI: 10.1016/j.cartre.2023.100276.
6 F. Yuan, Z. Wang, X. Li, Y. Li, Z. Tan, L. Fan and S. Yang, Bright Multicolor Bandgap Fluorescent Carbon Quantum Dots for Electroluminescent Light-Emitting Diodes, *Adv. Mater.*, 2017, **29**, 1604436, DOI: 10.1002/adma.201604436.
7 L. Wang, S. J. Zhu, H. Y. Wang, S. N. Qu, Y. L. Zhang, J. H. Zhang, Q. D. Chen, H. L. Xu, W. Han, B. Yang and H. B. Sun, Common origin of green luminescence in carbon nanodots and graphene quantum dots, *ACS Nano*, 2014, **8**, 2541–2547, DOI: 10.1021/nn500368m; P. Yu, X. Wen, Y.-R. Toh and J. Tang, Temperature-Dependent Fluorescence in Carbon Dots, *J. Phys. Chem. C*, 2012, **116**, 25552–25557, DOI: 10.1021/jp307308z.
8 P. K. Yadav, S. Chandra, V. Kumar, D. Kumar and S. H. Hasan, Carbon Quantum Dots: Synthesis, Structure, Properties, and Catalytic Applications for Organic Synthesis, *Catalysts*, 2023, **13**, 422, DOI: 10.3390/catal13020422.
9 E. M. Khalaf, N. A. Abood, R. Z. Atta, R.-A. A. Ramírez-Coronel, R. Alazragi, R. M. Romero Parra, O. H. Abed, M. Abosaooda, A. T. Jalil, Y. F. Mustafa, A. Narmani and B. Farhood, Recent progressions in biomedical and pharmaceutical applications of chitosan nanoparticles: A comprehensive review, *Int. J. Biol. Macromol.*, 2023, **231**, 123354, DOI: 10.1016/j.ijbiomac.2023.123354.
10 X. Li, D. Zeng, P. Ke, G. Wang and D. Zhang, Synthesis and characterization of magnetic chitosan microspheres for drug delivery, *RSC Adv.*, 2020, **10**, 7163, DOI: 10.1039/C9RA10792D.
11 B. Tian and J. Liu, Smart stimuli-responsive chitosan hydrogel for drug delivery: A review, *Int. J. Biol. Macromol.*, 2023, **235**, 123902, DOI: 10.1016/j.ijbiomac.2023.123902.
12 P. Grzybek, L. Jakubski and G. Dudek, Neat Chitosan Porous Materials: A Review of Preparation, Structure Characterization and Application, *Int. J. Mol. Sci.*, 2022, **23**, 9932, DOI: 10.3390/ijms23179932.
13 M. Ul-Islam, K. F. Alabbosh, S. Manan, S. Khan, F. Ahmad and M. W. Ullah, Chitosan-Based Nanostructured Biomaterials: Synthesis, Properties, and Biomedical Applications, *Adv. Ind. Eng. Polym. Res.*, 2024, **7**, 79, DOI: 10.1016/J.AIEPR.2023.07.002.
14 A. M. Villalba-Rodríguez, R. B. González-González, M. Martínez-Ruiz, E. A. Flores-Contreras, M. F. Cárdenas-Alcaide, H. M. N. Iqbal and R. Parra-Saldívar, Chitosan-Based Carbon Dots with Applied Aspects: New Frontiers of International Interest in a Material of Marine Origin, *Mar. Drugs*, 2022, **20**, 782, DOI: 10.3390/md20120782.
15 G. M. L. Consoli, M. L. Giuffrida, C. Satriano, T. Musumeci, G. Forte and S. Petralia, A novel facile one-pot synthesis of photothermally responsive carbon polymer dots as promising drug nanocarriers, *Chem. Commun.*, 2022, **58**, 3126, DOI: 10.1039/D1CC06530K.
16 G. M. L. Consoli, M. L. Giuffrida, S. Zimbone, L. Ferreri, L. Maugeri, M. Palmieri, C. Satriano, G. Forte and S. Petralia, Green Light-Triggerable Chemo-Photothermal Activity of Cytarabine-Loaded Polymer Carbon Dots: Mechanism and Preliminary In Vitro Evaluation, *ACS Appl. Mater. Interfaces*, 2023, **15**, 5732, DOI: 10.1021/acsami.2c22500.
17 N. Musso, P. G. Bonacci., G. M. L. Consoli, L. Maugeri, M. Terrana, L. Lanzanò, E. Longo, G. Buscarino, A. Consoli and S. Petralia, Biofriendly glucose-derived carbon nanodots: GLUT2-mediated cell internalization for an efficient targeted drug delivery and light-triggered cancer cell damage, *J. Coll. Interf. Sci.*, 2025, **696**, 137873, DOI: 10.1016/j.jcis.2025.137873.
18 S. Cho, H. Kim, D. Song, J. Jung, S. Park, H. Jo, S. Seo, C. Han, S. Park, W. Kwon and H. Han, Insights into glucose-derived carbon dot synthesis *via* Maillard reaction: from reaction mechanism to biomedical applications, *Sci. Rep.*, 2024, **14**, 31325, DOI: 10.1038/s41598-024-82767-z.
19 Z. Xing, Z. Ju, Y. Zhao, J. Wan, Y. Zhu, Y. Qiang and Y. Qian, One-pot hydrothermal synthesis of Nitrogen-doped graphene as high-performance anode materials for lithium ion batteries, *Sci. Rep.*, 2016, **6**, 26146, DOI: 10.1038/srep26146.
20 J. Jumardin, A. Maddu, K. Santoso and I. Isnaeni, Synthesis of carbon dots (cds) and determination of optical gap energy with Tauc plot method, *Jambura Phys. J.*, 2021, **3**, 73, DOI: 10.34312/jpj.v3i2.11235.
21 A. Hirai, H. Odani and A. Nakajima, Determination of degree of deacetylation of chitosan by 1H NMR spectroscopy, *Polym. Bull.*, 1991, **26**, 87, DOI: 10.1007/BF00299352.
22 T. Bhattacharjee, S. Rahman, D. Deka, M. K. Purkait, D. Chowdhury and G. Majumdar, Synthesis and characterization of exfoliated beta-cyclodextrin functionalized graphene oxide for adsorptive removal of atenolol, *Mat. Chem. Phys.*, 2022, **288**, 126413, DOI: 10.1016/j.matchemphys.2022.126413.
23 A. Gulino, G. G. Condorelli, P. Mineo and I. Fragalà, An x-ray photo electron spectra and atomic force microscopy characterization of silica substrates engineered with a covalently assembled siloxane monolayer, *Nanotechnology*, 2005, **16**, 2170–2175, DOI: 10.1088/0957-4484/16/10/033.
24 C. Rahmatunnisa, R. I. Chaerun, C. S. Budi and N. S. Gultom, Transforming Chitosan into N-Doped Carbon for Efficient CO2 Capture: A comprehensive Review, *Appl. Surf. Sci. Adv.*, 2025, **27**, 100774, DOI: 10.1016/j.apsadv.2025.100774.
25 A. Gulino, G. G. Condorelli, P. Mineo and I. Fragalà, An x-ray photo electron spectra and atomic force microscopy characterization of silica substrates engineered with a covalently assembled siloxane monolayer, *Nanotechnology*, 2005, **16**, 2170–2175, DOI: 10.1088/0957-4484/16/10/033.
26 A. Gulino, F. Lupo, G. G. Condorelli, M. E. Fragalà, M. E. Amato and G. Scarlata, Reversible photoswitching of

stimuli-responsive Si(100) surfaces engineered with an assembled 1-cyano-1-phenyl-2-[4′-(10-undecenyloxy)phenyl]-ethylene monolayer, *J. Mater. Chem.*, 2008, **18**, 5011–5018, DOI: 10.1039/B809037H.

27 A. Kumar, M. Chhatwal, P. C. Mondal, V. Singh, D. A. Cristaldi, R. D. Gupta and A. Gulino, Ternary Memory Module Using Low-Voltage Control over Optical Properties of Metal- Polypyridyl Monolayers, *Chem. Commun.*, 2014, **50**, 3783–3785, DOI: 10.1039/C4CC00388H.

28 S. A. Mathew, P. Praveena, S. Dhanavel, R. Manikandan, S. Senthilkumar and A. Stephen, Luminescent chitosan/carbon dots as an effective nano-drug carrier for neurodegenerative diseases, *RSC Adv.*, 2020, **10**, 24386, DOI: 10.1039/D0RA04599C.

29 X. Liu, J. Pang, F. Xu and X. Zhang, Simple Approach to Synthesize Amino-Functionalized Carbon Dots by Carbonization of Chitosan, *Sci. Rep.*, 2016, **6**, 31100, DOI: 10.1038/srep31100.

30 D. Li, K. Huang, J. She, Y. Cai, B. Liu, Z. Wei, Y. Chen, J. Huang and H. Fan, Two-photon fluorescence-guided precise photothermal therapy located in a single cancer cell utilizing bifunctional N-doped carbon quantum dots, *J. Coll. Interf. Sci.*, 2024, **15**, 719–726, DOI: 10.1016/j.jcis.2024.02.114.

31 G. M. L. Consoli, L. Maugeri, G. Forte, G. Buscarino, A. Gulino, L. Lanzanò, P. Bonacci, N. Musso and S. Petralia, Red light-triggerable nanohybrids of graphene oxide, gold nanoparticles and thermo-responsive polymers for combined photothermia and drug release effects, *J. Mater. Chem. B*, 2024, **12**, 952–961, DOI: 10.1039/D3TB01863F.

32 R. M. Chiechio, S. Ducarre, G. Moulin, A. Dupont, C. Marets, P. Even-Hernandez, F. Artzner, P. Musumeci, G. Franzò, C. Ravel, M. J. LoFaro and V. Marchi, Luminescent Gold Nanoclusters Interacting With Synthetic and Biological Vesicles, *J. Phys. Chem. Lett.*, 2022, **13**, 6935, DOI: 10.1021/acs.jpclett.2c01071.

33 R. M. Chiechio, A. Scandurra, R. Reitano, P. Musumeci, M. G. Grimaldi, A. Contino, G. Maccarrone, V. Marchi, L. Maugeri, S. Petralia and F. Ruffino, Quantum fluorescent gold nanoclusters for PCR-free ultrasensitive DNA detection, *Appl. Surf. Sci. Adv.*, 2025, **27**, 100762, DOI: 10.1016/j.apsadv.2025.100762.

34 N. Duraisamy, S. Dhayalan, M. R. Shaik, A. H. Shaik, J. P. Shaik and B. Shaik, Green Synthesis of Chitosan Nanoparticles Using of Martynia annua L. Ethanol Leaf Extract and Their Antibacterial Activity, *Crystals*, 2022, **12**, 1550, DOI: 10.3390/cryst12111550.

35 G. M. L. Consoli, L. Maugeri, N. Musso, A. Gulino, L. D'Urso, P. Bonacci, G. Buscarino, G. Forte and S. Petralia, One-pot synthesis of luminescent and photothermal carbon boron-nitride quantum dots exhibiting cell damage protective effects, *Adv. Healthcare Mater.*, 2024, **13**, e2303692, DOI: 10.1002/adhm.202303692.

36 D. E. Johnson, R. A. O'Keefe and J. R. Grandis, Targeting the IL-6/JAK/STAT3 signalling axis in cancer, *Rev. Clin. Oncol.*, 2018, **15**, 234, DOI: 10.1038/nrclinonc.2018.8.

37 M. J. Dehzad, H. Ghalandari, M. Nouri and M. Askarpour, Antioxidant and anti-inflammatory effects of curcumin/turmeric supplementation in adults: A GRADE-assessed systematic review and dose-response meta-analysis of randomized controlled trials, *Cytokine*, 2023, **164**, 156144, DOI: 10.1016/j.cyto.2023.156144.

38 N. Kumari, B. S. Dwarakanath, A. Dasand and A. N. Bhatt, Role of interleukin-6 in cancer progression and therapeutic resistance, *Tumour Biol.*, 2016, **37**, 11553, DOI: 10.1007/s13277-016-5098-7.

39 D. Chowdhury, N. Gogoia and G. Majumdarb, Fluorescent carbon dots obtained from chitosan gel, *RSC Adv.*, 2012, **2**, 12156–12159, DOI: 10.1039/C2RA21705H.

40 M. Omidi, A. Yadegari and L. Tayebi, Wound dressing application of pH-sensitive carbon dots/chitosan hydrogel, *RSC Adv.*, 2017, **7**, 10638–10649, DOI: 10.1039/C6RA25340G.

41 A. Konwar, N. Gogoi, G. Majumdar and D. Chowdhurya, Green chitosan-carbon dots nanocomposite hydrogel film with superior properties, *Carbohydr. Polym.*, 2015, **115**, 238–245, DOI: 10.1016/j.carbpol.2014.08.021.

42 X. Liu, J. Pang, F. Xu and X. Zhang, Simple Approach to Synthesize Amino-Functionalized Carbon Dots by Carbonization of Chitosan, *Sci. Rep.*, 2016, **6**, 31100, DOI: 10.1038/srep31100; T. Sarkar, H. B. Bohidar and R. P. Solanki, Carbon dots-modified chitosan based electrochemical biosensing platform for detection of vitamin D, *Intern. J. Biol. Macromol.*, 2018, **109**, 687–31697, DOI: 10.1016/j.ijbiomac.2017.12.122.

43 S. A. Mathew, P. Praveena, S. Dhanavel, R. Manikandan, S. Senthilkumar and A. Stephen, Luminescent chitosan/carbon dots as an effective nano-drug carrier for neurodegenerative diseases, *RSC Adv.*, 2020, **10**, 24386–24396, DOI: 10.1039/d0ra04599c.

44 S. K. Paliwal, D. Sarkar, A. Mitra and V. Mahalingam, Chitosan-Derived N-Doped Carbon for Light-Mediated Carbon Dioxide Fixation into Epoxides, *ChemPlusChem*, 2023, **88**, e202300448, DOI: 10.1002/cplu.202300448.

45 L. Sun, H. Zhang, Y. Wang, Z. Xiong, X. Zhao and Y. Xia, Chitosan-derived N-doped carbon dots for fluorescent determination of nitrite and bacteria imaging, *Mol. Biomol. Spectrosc.*, 2021, **251**, 119468, DOI: 10.1016/j.saa.2021.119468.

46 S. Kariminia, M. Shamsipur and A. Barati, Fluorescent folic acid-chitosan/carbon dot for pH-responsive drug delivery and bioimaging, *Int. J. Biol. Macromol.*, 2024, **254**, 127728, DOI: 10.1016/j.ijbiomac.2023.127728.

47 S. Chen, Q. Zeng, X. Tan, M. Ye, Y. Zhang, L. Zou, S. Liu, Y. Yang, A. Liu, L. He and K. Hu, Photodynamic antibacterial chitosan/nitrogen-doped carbon dots composite packaging film for food preservation applications, *Carbohy. Polym.*, 2023, **314**, 120938, DOI: 10.1016/j.carbpol.2023.120938.

48 Z. Yang, M. Xu, Y. Liu, F. He and Y. Gao, Controllable Synthesis of Fluorescent Carbon Dots and Their Detection Application as Nanoprobes, *Nano-Micro Lett.*, 2013, **5**, 247–259, DOI: 10.1007/BF03353756.

49 D. Briggs, J. T. Grant, *Surface Analysis by Auger and X-Ray Photoelectron Spectroscopy*, IM Pub, Chichester, UK, 2003, ISBN 1-901019-04-7/978-1901019049;; A. Gulino, G. G. Condorelli, P. Mineo and M. E. Fragalà, Structural and electronic characterization of self-assembled molecular nanoarchitectures by X-ray photoelectron spectroscopy, *Anal. Bioanal. Chem.*, 2013, **405**, 1479–1495, DOI: 10.1007/s00216-012-6394-8.

50 G. Greczynski and L. Hultman, Compromising Science by Ignorant Instrument Calibration – Need to Revisit Half a Century of Published XPS, *Angew. Chem.*, 2020, **59**, 5002–5006, DOI: 10.1002/anie.201916000.

51 G. Granata, S. Petralia, G. Forte, S. Conoci and G. M. L. Consoli, Injectable supramolecular nanohydrogel from a micellar self-assembling calix[4]arene derivative and curcumin for a sustained drug release, *Mater. Sci. Eng. C*, 2020, **111**, 110842, DOI: 10.1016/j.msec.2020.110842.

52 G. Consiglio, S. Failla, C. G. Fortuna, L. D'Urso and G. Forte, Aggregation of a Zn(II)-salen complex: Theoretical study of structure and spectra, *Comput. Theor. Chem.*, 2015, **1067**, 1, DOI: 10.1016/j.comptc.2015.05.014.

53 S. Grimme, Accurate description of van der Waals complexes by density functional theory including empirical corrections, *Comput. Chem.*, 2004, **25**, 1463, DOI: 10.1002/jcc.20078.

54 M. Cossi, N. Rega, G. Scalmani and V. Barone, Energies, structures, and electronic properties of molecules in solution with the C-PCM solvation model, *J. Comput. Chem.*, 2003, **24**, 669, DOI: 10.1002/jcc.10189.

55 T. Yanai, D. P. Tew and N. C. Handy, A new hybrid exchange-correlation functional using the Coulomb-attenuating method (CAM-B3LYP), *Chem. Phys. Lett.*, 2004, **393**, 51–57, DOI: 10.1016/j.cplett.2004.06.011.